optics

MDPI

Article

Temporal Cavity Soliton Interaction in Passively Mode-Locked Semiconductor Lasers

Andrei G. Vladimirov

Weierstrass Institute, Mohrenstr. 39, 10117 Berlin, Germany; andrei.vladimirov@wias-berlin.de

Abstract: Weak interactions of temporal cavity solitons resulting from gain saturation and recovery in a delay differential model of a long cavity semiconductor laser were studied numerically and analytically using an asymptotic approach. This paper shows that in addition to the usual soliton repulsion leading to a harmonic mode-locking regime, soliton attraction is also possible in a laser with a nonzero linewidth enhancement factor. It is shown numerically that this attraction can lead either to pulse merging or to pulse bound-state formation.

Keywords: mode-locking; semiconductor laser; delay differential equation model; temporal cavity solitons

check for updates

Citation: Vladimirov, A.G. Temporal Cavity Soliton Interaction in Passively Mode-Locked Semiconductor Lasers. *Optics* **2023**, *4*, 433–446. https://doi.org/10.3390/opt4030031

Academic Editor: Clare C. Byeon

Received: 14 June 2023
Revised: 2 July 2023
Accepted: 13 July 2023
Published: 26 July 2023

1. Introduction

Temporal cavity solitons (TCSs) are short nonlinear optical pulses generated by mode-locked lasers and optical microresonators that preserve their shape in the course of propagation [1–3]. In lasers, unlike the usual self-starting mode-locked pulses generated above the linear laser threshold, TCSs coexist with a stable laser off regime and require a finite perturbation for their excitation. For example, when the cavity length of a laser with a semiconductor gain medium is sufficiently large, usual mode-locked pulses can be transformed into TCSs [4], corresponding to a non-self-starting mode-locking regime. In many practical situations, when more than one TCS is exited in an optical cavity, weak interactions among the TCSs may take place via their exponentially decaying tails. Spatial and temporal dissipative soliton interaction in lasers with saturable absorbers have been studied in many publications in cases in which the gain and absorption variables are eliminated adiabatically and interactions take place only via the overlapping electric fields of the pulses [5–10]. The interaction of mode-locked pulses in the presence of finite relaxation times of the gain and/or absorber media has been less investigated. In this case, the electromagnetic field saturates gain and absorption behind the pulse, and their slow relaxation can affect the position of the next pulse traveling in the cavity. This type of interaction was studied in refs. [11–15]. In particular, it was demonstrated theoretically and verified experimentally with solid state and fiber lasers [11] that the interaction due to gain depletion and very slow recovery can produce a repulsive force between adjacent pulses, leading to the formation of a harmonic mode-locking regime. A similar conclusion was made in ref. [13] using the delay differential equation (DDE) model [16–18] of a mode-locked monolithic semiconductor laser, where similarly to ref. [11], the gain recovery time was much longer than the cavity round-trip time. Here, using the same DDE model, I consider mode-locked pulse interaction in the TCS regime, where the cavity round-trip time is sufficiently long—much longer than the gain recovery time. Based on an asymptotic approach, the equations governing the slow evolution of the time separation and phase difference of the interacting TCSs are derived and analyzed. Asymptotic study of weak TCS interactions in DDE models of optical systems has already been previously carried out in [19–21]. However, in ref. [21], devoted to TCS interaction in nonlinear mirror mode-locked lasers, and in this paper, a closed analytical form of the interaction equations is derived. Furthermore, among the above-cited works, only refs. [13,15] are devoted to pulse interactions in semiconductor lasers. However, in ref. [13], a short cavity laser operating far away from the TCS regime is considered, while the analysis in ref. [15] is more or less empirical. Therefore, a more rigorous analysis of TCS interactions in semiconductor lasers that takes into account their characteristic features, such as the linewidth enhancement factor, is required. This work aimed to fill in this gap. Using interaction equations, I show that the TCS interaction scenarios depend on the "interaction coefficients" introduced below and can be more rich than those described in [11,13,15]. In addition to the pulse repulsion resulting in a harmonic mode-locking regime, TCS attraction leading to either pulse merging or bound-state formation can take place in a laser with a nonzero linewidth enhancement factor. Note that soliton attraction leading to bound-state formation was previously observed in ref. [12] in a complex Ginzburg–Landau equation-type mode-locked laser model with second-order dispersion and in the DDE model of a nonlinear mirror mode-locked laser [21]. However, unlike the present work, where the mode-locking mechanism is due to the interplay of gain and absorption saturation and recovery [16], in both those papers, Kerr nonlinearity played a decisive role in the process of mode-locked pulse formation. Furthermore, since ref. [12] considered the limit of infinitely large gain recovery time, the mechanism of pulse interaction in this paper is different and can be attributed to the saturation and slow recovery of absorption rather than gain. The results of this work might be useful for pulse spacing manipulation in multipulse mode-locked lasers.

2. Model Equations

The DDE model of a passively mode-locked semiconductor laser for the electric field amplitude ($A(t)$) at the entrance of the laser absorber section, the saturable gain ($G(t)$), and the saturable absorption ($Q(t)$), can be written in the form [16–18]:

$$\gamma^{-1}\partial_t A + (1 + i\omega)A = R(t - T)A(t - T), \tag{1}$$

$$\partial_t G = g_0 - \gamma_g G - e^{-Q}\left(e^G - 1\right)|A|^2, \tag{2}$$

$$\partial_t Q = q_0 - \gamma_q Q - s\left(1 - e^{-Q}\right)|A|^2, \tag{3}$$

with

$$R(t) = \sqrt{\kappa}e^{(1-i\alpha_g)G(t)/2-(1-i\alpha_q)Q(t)/2+i\phi-i\omega T}.$$

where t is the time variable; κ is the attenuation factor describing linear non-resonant intensity losses per cavity round trip; and α_g and α_q are the linewidth enhancement factors in the gain and absorber sections, respectively. The time delay parameter (T) stands for the cold cavity round-trip time; γ is the spectral filtering bandwidth; γ_g and γ_q are the normalized carrier relaxation rates in the gain and absorber sections; and s is the ratio of the saturation intensities of these sections. The pump parameter (g_0) depends on the injection current in the gain section, while q_0 is the unsaturated loss parameter, which depends on the inverse voltage applied to the absorber section. Parameter ϕ is the phase shift describing the detuning between the central frequency of the spectral filter and the closest cavity mode and ω is the reference frequency.

It is well known that in a certain parameter domain, Equations (1)–(3) demonstrate pulsed solutions corresponding to fundamental single pulse and harmonic multipulse mode-locking regimes [16–18]. Furthermore, it was shown in [4] that when the laser cavity is sufficiently long that the round-trip time is much larger than the gain relaxation time, these pulses can be transformed into TCSs sitting on the stable laser off solution. In this situation, two well-separated mode-locking pulses can interact only weakly via their exponentially decaying tails. Furthermore, when the pulses are sufficiently far away from one another, this interaction is mainly due to the gain component (G), which usually decays much slower than the electric field envelope (A) and saturable absorption (Q). Note, however, that when the distance between the TCSs becomes small enough, the interaction via absorption dynamics might also come into play and even lead to pulse bound-state formation; see ref. [12], where the case of infinitely large gain recovery time is considered.

In order to derive the TCS interaction equations, we rewrite the model equations in a more general real vector form

$$\partial_t \mathbf{U} = \mathbf{F}_\omega(\mathbf{U}) + \mathbf{H}_\omega[\mathbf{U}(t-T)], \tag{4}$$

where $\mathbf{U} = \begin{pmatrix} U_1 & U_2 & U_3 & U_4 \end{pmatrix}^T$ is the real column vector with the components $U_1 = \Re A$, $U_2 = \Im A$, $U_3 = G - g_0/\gamma_g$, and $U_4 = Q - q_0/\gamma_q$. The two vectors in the right-hand side of Equation (4) are defined by

$$\mathbf{F}_\omega(\mathbf{U}) = \begin{pmatrix} -\gamma(U_1 - \omega U_2) \\ -\gamma(U_2 + \omega U_1) \\ -\gamma_g U_3 - e^{-U_4 - q_0/\gamma_q}\left(e^{U_3 + g_0/\gamma_g} - 1\right)(U_1^2 + U_2^2) \\ -\gamma_q U_4 - s\left(1 - e^{-U_4 - q_0/\gamma_q}\right)(U_1^2 + U_2^2) \end{pmatrix},$$

and

$$\mathbf{H}_\omega(\mathbf{U}) = \begin{pmatrix} -\Re[R(U_1 + iU_2)] \\ -\Im[R(U_1 + iU_2)] \\ 0 \\ 0 \end{pmatrix}$$

with

$$R(t) = \gamma\sqrt{\kappa} e^{(1-i\alpha_g)\left(U_3 + g_0/\gamma_g\right)/2 - (1-i\alpha_q)\left(U_4 + q_0/\gamma_q\right)/2 - i\omega T}.$$

3. Temporal Cavity Soliton

Let us assume that the relation

$$\gamma^{-1} < \gamma_q^{-1} < \gamma_g^{-1} \ll T, \tag{5}$$

for the relaxation rates in the model Equations (1)–(3) is satisfied. This means that the round trip time in a multimode semiconductor laser cavity is sufficiently long, much longer than the gain relaxation time. In this case, the DDE model can have TCS solutions [4]. Let $\mathbf{U} = \mathbf{u} = \begin{pmatrix} u_1 & u_2 & u_3 & u_4 \end{pmatrix}^T$ and $\omega = \omega_0$ be a TCS solution of Equation (4) corresponding to a narrow mode-locked pulse with the duration $\tau_p \sim \gamma^{-1}$. Here, $\mathbf{u}(t) = \mathbf{u}(t + T_0)$ is periodic in time with the period T_0 close to the delay time T. In terms of the original model Equations (1)–(3) we have

$$\mathbf{u} = \begin{bmatrix} \Re A_0(t) & \Im A_0(t) & G_0(t) - g_0/\gamma_g & Q_0(t) - q_0/\gamma_q \end{bmatrix}^T,$$

where $A_0(t)$, $G_0(t)$, and $Q_0(t)$ is a T_0-periodic TCS solution of these equations. A numerically calculated intensity time trace of the TCS solution is shown in Figure 1a.

The decay rates of the TCS tails are determined by the following linearization [22–24] of Equation (4) on the solution $\mathbf{U} = 0$:

$$\gamma^{-1}\partial_t a + (1 + i\omega_0)a = R_0 a(t + \delta), \tag{6}$$

$$\partial_t v_3 = -\gamma_g v_3. \tag{7}$$

$$\partial_t v_4 = -\gamma_q v_4, \tag{8}$$

where $a = v_1 + iv_2$, $\mathbf{v} = \begin{pmatrix} v_1 & v_2 & v_2 & v_4 \end{pmatrix}^T$ is a small perturbation vector,

$$R_0 = \sqrt{\kappa} e^{(1-i\alpha_g)g_0/(2\gamma_g) - (1-i\alpha_q)q_0/(2\gamma_q) + i\phi + i\omega_0\delta},$$

and the time advance parameter is $\delta = T_0 - T$. It follows from Equations (7) and (8) that the decay rates of the TCS gain and absorption components at large positive times t are determined by the two eigenvalues $\lambda_{g,q} = -\gamma_{g,q}$, while Equation (6) has an infinite number of eigenvalues defined by

$$\lambda_k = -\gamma(1 + i\omega_0) - \delta^{-1} W_k \left[-\gamma\delta e^{-(1+i\omega_0)\gamma\delta} R_0 \right]. \tag{9}$$

here W_k is the Lambert function with the index $k = 0, \pm 1, \pm 2 \ldots$. For the parameter values of Figure 1 we get $\lambda_0 = -3.741$ and $\lambda_{-1} = 16.892$, while all the other eigenvalues are complex and have positive real parts greater than λ_{-1}.

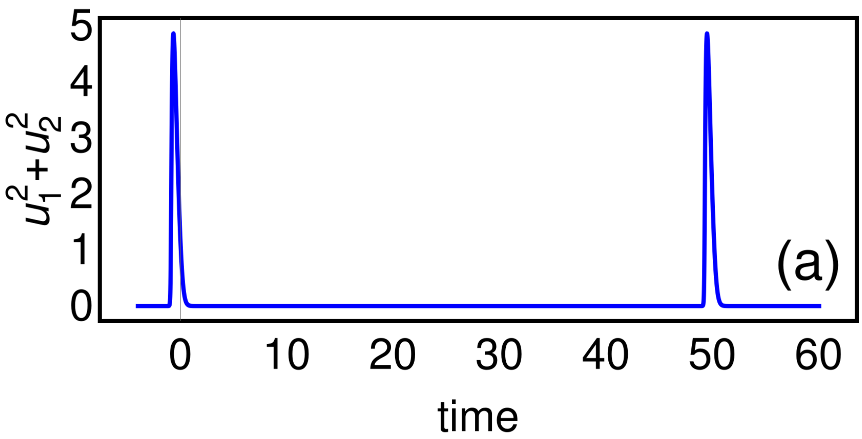

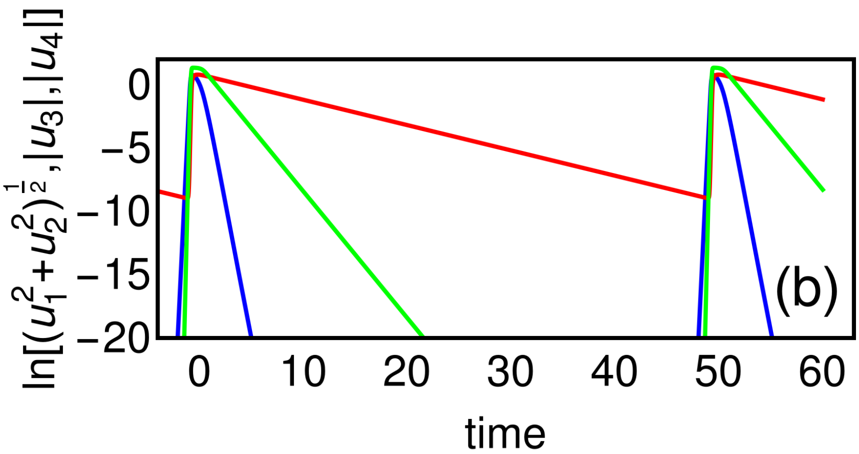

Figure 1. Intensity time trace of the periodic TCS solution of Equations (1)–(3) (**a**). Temporal evolution of the logarithm of the absolute values of the field envelope (blue), gain (red) and loss (green) components of the TCS solution (**b**). The parameters are: $\alpha_g = \alpha_q = 0$, $g_0 = 0.5$, $q_0 = 4.0$, $\kappa = 0.8$, $s = 10.0$, $\gamma = 5.0$, $\gamma_g = 0.2$, $\gamma_q = 1.0$, and $T = 50.0$. The solution period is $T_0 = 50.138425$ and $\omega_0 = 0$.

Assuming that the origin of the time coordinate, $t = 0$, is located at the TCS power peak, we determine based on (7)–(9) that at sufficiently large $t > 0$ the TCS trailing edge can be represented as

$$u_{1,2} \sim b_{1,2} e^{\lambda_0 t}, \quad u_3 \sim b_3 e^{-\gamma_g t}, \quad u_4 \sim b_4 e^{-\gamma_q t}, \tag{10}$$

where $b_{1,2,3,4}$ are real constants, which can be calculated numerically.

Further, let us consider the leading tail of the TCS at negative times, $t < 0$. Since Equations (7) and (8) have no eigenvalues with positive real parts, gain and absorption components of the TCS leading edge, u_3 and u_4, decay faster than exponentially in negative time [22]. The field component $u_1 + iu_2$ of the leading tail decays exponentially at $t < 0$, with the decay rate determined by the eigenvalue λ_{-1} having the smallest positive real part. Since the inequality $\gamma_{g,q} < |\lambda_0| < \lambda_{-1}$ is satisfied, the field component of the TCS decays faster in both time directions than the gain and absorption components in positive time. This means that the interaction via the electromagnetic field dynamics can be neglected when considering the interaction of two well-separated TCSs. Such a type of interaction is typical of lasers with slow gain and absorption and can be viewed as the long-range interaction [21], in contrast with the short-range interaction due to the overlap of the electric fields considered in [5–9,25]. Furthermore, since gain and absorption components of a TCS decay faster than exponentially in negative time, the leading tails of the TCSs can be neglected in the derivation of the interaction equations. Figure 1b shows the time evolution of the absolute values of field envelope $\sqrt{U_{01}^2 + U_{02}^2}$, gain $|U_{03}|$, and absorption $|U_{04}|$ components of this solution in logarithmic scale. It is seen from this figure that the gain component dominates over the field and absorption ones during almost the whole time interval between the two consequent pulses.

The stability of the TCS depends on the spectrum of the linear operator $\mathcal{L}$ obtained via linearization of Equation (4) at the solution $\mathbf{U} = \mathbf{u}$ and $\omega = \omega_0$. Since the model Equations (1)–(3) are invariant under time translations, $\mathbf{U}(t) \to \mathbf{U}(t - t_0)$, and phase shifts, $U_1 + iU_2 \to (U_1 + iU_2)e^{i\phi_0}$, with arbitrary constants t_0 and ϕ_0, the operator $\mathcal{L}$ has two zero eigenvalues corresponding to the neutral (Goldstone) modes given by $\boldsymbol{\theta} = \partial_t \mathbf{u}$ and $\boldsymbol{\varphi} = \begin{pmatrix} -u_2 & u_1 & 0 & 0 \end{pmatrix}^T$, respectively, $\mathcal{L}\boldsymbol{\theta} = -\partial_t \boldsymbol{\theta} + \mathcal{B}\boldsymbol{\theta} + \mathcal{C}_T \boldsymbol{\theta}(t - T) = 0$ and $\mathcal{L}\boldsymbol{\varphi} = 0$. Here, $\mathcal{B} = \mathcal{B}(\mathbf{u})$ and $\mathcal{C}_T = \mathcal{C}[\mathbf{u}(t - T)]$ are the linearization matrices of $\mathbf{F}_{\omega_0}(\mathbf{U})$ and $\mathbf{H}_{\omega_0}[\mathbf{U}(t - T)]$ at $\mathbf{U} = \mathbf{u}$. Below, it is assumed that the TCS is stable and the rest of the spectrum of the operator $\mathcal{L}$ is located in the left half of the complex plane. The adjoint linear operator $\mathcal{L}^\dagger$ also has two zero eigenvalues associated with the so-called adjoint neutral modes $\boldsymbol{\theta}^\dagger$ and $\boldsymbol{\varphi}^\dagger$, $\mathcal{L}^\dagger \boldsymbol{\theta}^\dagger = \partial_t \boldsymbol{\theta}^\dagger + \boldsymbol{\theta}^\dagger \mathcal{B} + \boldsymbol{\theta}^\dagger (t + T)\mathcal{C} = 0$ and $\mathcal{L}^\dagger \boldsymbol{\varphi}^\dagger = 0$. Let the adjoint neutral modes be biorthogonal to the neutral modes, $\left\langle \boldsymbol{\theta}^\dagger \cdot \boldsymbol{\varphi} \right\rangle = \langle \boldsymbol{\varphi}^\dagger \cdot \boldsymbol{\theta} \rangle = 0$ and $\left\langle \boldsymbol{\theta}^\dagger \cdot \boldsymbol{\theta} \right\rangle = \langle \boldsymbol{\varphi}^\dagger \cdot \boldsymbol{\varphi} \rangle = 1$, where $\langle \boldsymbol{x}^\dagger \cdot \boldsymbol{y} \rangle = \int_0^{\tau_0} \boldsymbol{x}^\dagger \cdot \boldsymbol{y} dt$. Asymptotic behavior of the row vector adjoint neutral modes $\boldsymbol{\theta}^\dagger = \begin{pmatrix} \theta_1^\dagger & \theta_2^\dagger & \theta_3^\dagger & \theta_4^\dagger \end{pmatrix}$ and $\boldsymbol{\varphi}^\dagger = \begin{pmatrix} \varphi_1^\dagger & \varphi_2^\dagger & \varphi_3^\dagger & \varphi_4^\dagger \end{pmatrix}$ at sufficiently large negative times $t < 0$ is given by

$$\theta_{1,2}^\dagger \sim c_{1,2} e^{-\lambda_0 t}, \quad \theta_3^\dagger \sim c_3 e^{\gamma_g t}, \quad \theta_4^\dagger \sim c_4 e^{\gamma_q t}, \tag{11}$$

$$\varphi_{1,2}^\dagger \sim d_{1,2} e^{-\lambda_0 t}, \quad \varphi_3^\dagger \sim d_3 e^{\gamma_g t}, \quad \varphi_4^\dagger \sim d_4 e^{\gamma_q t}, \tag{12}$$

where $c_{1,2,3,4}$ and $d_{1,2,3,4}$ are real coefficients, which can be calculated numerically. Similar to the leading tail of the TCS solution, the gain and absorption components of the trailing tail of the adjoint neutral modes decay faster than exponentially at $t > 0$. Therefore, trailing tails of the adjoint neutral modes can be neglected in the derivation of the interaction equations. The temporal evolution of the field, gain, and loss components of the translational adjoint neutral mode $\boldsymbol{\theta}^\dagger = \begin{pmatrix} \theta_1^\dagger & \theta_2^\dagger & \theta_3^\dagger & \theta_4^\dagger \end{pmatrix}$ are shown in Figure 2. One can see that, similar to Figure 1, the gain component $\theta_3^\dagger$ of the adjoint neutral mode dominates almost everywhere between the consequent mode-locked pulses. Therefore, one can conclude that the pulse interaction via the field and absorption dynamics can be neglected for the parameter values of these figures.

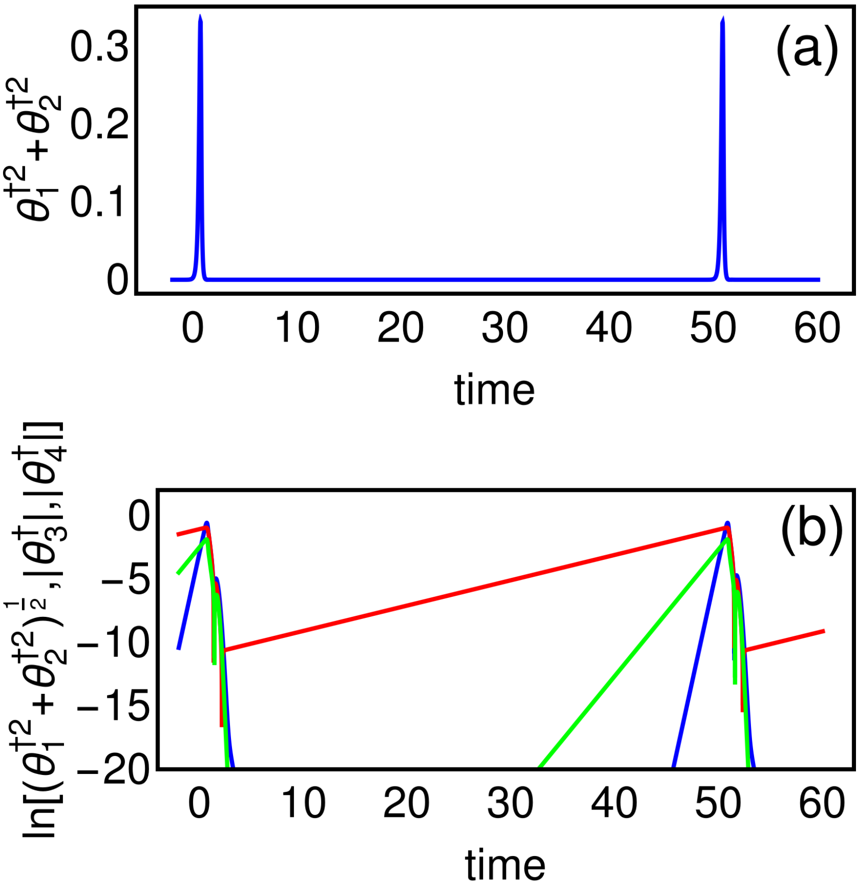

Figure 2. Field intensity of the adjoint neutral mode $\boldsymbol{\theta}^\dagger$ as a function of time (**a**). Temporal evolution of the logarithm of the absolute values of the field (blue), gain (red), and loss (green) components of the translational adjoint neutral mode $\boldsymbol{\theta}^\dagger$ (**b**). Parameters are the same as in Figure 1.

4. Interaction Equations

To derive the equations describing slow evolution of the time coordinates and phases of weakly interacting TCSs, let us look for the solution of Equation (4) in the form of a sum of two unperturbed TCS solutions plus a small correction, $\mathbf{w}(\mathbf{t}) = \mathcal{O}(\epsilon)$, due to the interaction:

$$\mathbf{U} \;=\; \sum_{k=1}^{2} \mathbf{u}_k + \mathbf{w}, \tag{13}$$

where $\mathbf{u}_k = \begin{pmatrix} u_{1k} & u_{2k} & u_{3k} & u_{4k} \end{pmatrix}^T$ with $u_{1k} + iu_{2k} = [u_1(t-\tau_k) + iu_2(t-\tau_k)]e^{-i\phi_k}$, $u_{3k} = u_3(t-\tau_k)$, and $u_{4k} = u_4(t-\tau_k)$. Coordinates τ_k and phases ϕ_k of the interacting TCSs are assumed to be slow functions of time, $\partial_t\tau_k, \partial_t\phi_k = \mathcal{O}(\epsilon)$, $k = 1, 2$. The small parameter ϵ characterizes weak overlap of the TCSs. Similar to the case of dissipative soliton interaction in partial differential equation laser models [9,25–27], the right-hand side of the interaction equations obtained from our DDE model can be expressed in terms of the TCS solutions and their adjoint neutral modes evaluated at the point between the two TCSs [21]. The details of the calculations are given in the Appendix A, where it is shown that the interaction equations for the time separation $\Delta\tau = \tau_2 - \tau_1$ and phase difference $\Delta\phi = \phi_2 - \phi_1$ of a pair of interacting T_0-periodic TCS take the form

$$\partial_t\Delta\tau \approx \boldsymbol{\theta}_1^\dagger(T_0/2)\mathbf{u}_2(T_0/2) - \boldsymbol{\theta}_2^\dagger(0)\mathbf{u}_1(0), \tag{14}$$

$$\partial_t\Delta\phi \approx \boldsymbol{\varphi}_1^\dagger(T_0/2)\mathbf{u}_2(T_0/2) - \boldsymbol{\varphi}_2^\dagger(0)\mathbf{u}_1(0), \tag{15}$$

where $\boldsymbol{\theta}_k^\dagger = \boldsymbol{\theta}^\dagger(t - t_k)$ and $\boldsymbol{\varphi}_k^\dagger = \boldsymbol{\varphi}^\dagger(t - t_k)$ are the adjoint neutral modes evaluated at the kth TCS ($k = 1, 2$) and without loss of generality, one can assume that $t = 0$ and $t = T_0/2$ correspond, respectively, to the middle point between the two interacting TCSs and the opposite point on a circle with the circumference T_0.

Substituting asymptotic Expressions (10)–(12) into the interaction Equations (14) and (15) and neglecting the field components we get

$$\partial_t \Delta\tau = K_{\tau g}\left[e^{-\gamma_g(T_0-\Delta\tau)} - e^{-\gamma_g\Delta\tau}\right] + K_{\tau q}\left[e^{-\gamma_q(T_0-\Delta\tau)} - e^{-\gamma_q\Delta\tau}\right], \tag{16}$$

$$\partial_t \Delta\phi = K_{\phi g}\left[e^{-\gamma_g(T_0-\Delta\tau)} - e^{-\gamma_g\Delta\tau}\right] + K_{\phi q}\left[e^{-\gamma_q(T_0-\Delta\tau)} - e^{-\gamma_q\Delta\tau}\right] \tag{17}$$

with $K_{\tau g} = b_3c_3$, $K_{\tau q} = b_4c_4$, $K_{\phi g} = b_3d_3$, and $K_{\phi q} = b_4d_4$.

Interaction Equations (16) and (17) describe the long-range interaction of two well-separated TCS via gain and absorption dynamics and do not take into account the short-range interaction due to weak overlap of the electric field envelopes of the TCSs. They reflect the fact that in a ring cavity, the interaction of two TCSs is twofold. The trailing tail of the first (second) TCS overlaps with the leading tail of the adjoint neutral mode of the second (first) TCS, which is located at distance $\Delta\tau$ ($T_0 - \Delta\tau$) behind it. This is reflected by the presence of the two exponential terms in the square brackets of Equations (16) and (17). In the case of TCS repulsion ($K_{\tau g} < 0$), this type of twofold interaction leads to a regime with two equally spaced pulses per cavity round trip corresponding to a harmonic mode-locking regime. As I have already noted, due to the inequality $\gamma_q > \gamma_g$ typical of semiconductor lasers, the interaction force related to absorption dynamics decays much faster than that due to gain dynamics and the terms proportional to $K_{\tau q}$ and $K_{\phi q}$ can be neglected in the interaction equations.

5. Results of Numerical Simulations

For the parameter values of Figures 1 and 2 corresponding to zero linewidth enhancement factors, $\alpha_g = \alpha_q = 0$, numerically, we get $K_{\tau g} = -1.120$ and $K_{\tau q} = 2.145$ in Equation (16). Due to the relation $K_{\phi g} = K_{\phi q} = d_3 = d_4 = 0$, which is the consequence of $\omega_0 = \Im A_0 = 0$, the second interaction Equation (17) transforms into $\partial_t\Delta\phi = 0$. For negative values of $K_{\tau g}$ the TCS interaction is repulsive, while positive $K_{\tau q}$ corresponds to TCS attraction via absorption dynamics. However, as discussed above, for the parameter values of these figures, the interaction via gain dynamics dominates for almost all sufficiently large soliton separations, and the soliton attraction due to absorption dynamics is hardly possible to observe. The repulsive interaction is illustrated in Figure 3 obtained via numerical integration of Equations (1)–(3) using the RADAR5 code [28]. The initial condition was taken as a sum of two or more well-separated unperturbed TCSs. Figure 3a shows the standard mechanism of the harmonic mode-locking regime formation as a result of the repulsion of a pair of TCSs due to the interaction via gain dynamics. Figure 3b was obtained using the same parameter values as in Figure 3a, but with smaller initial separation of the two TCSs. It is seen that during the first stage of the interaction, there is still repulsion between the TCSs, but later, the second TCS becomes smaller and finally disappears. The equation $\partial_t\Delta\phi = 0$ implies that the TCS phase difference remains almost constant in the course of the interaction. This difference is affected only by a very weak overlap of the field components which were neglected in the derivation of the interaction Equations (16) and (17). Repulsive interaction of three and four TCSs leading to the development of harmonic mode-locking regimes with three and four pulses per cavity round trip is illustrated in Figure 3c and Figure 3d, respectively. Here, the transformation of a train of initially non-equidistant pulses into an equidistant pulse train clearly indicates the repulsive nature of the interaction. Note that in order to produce Figure 3 with minimized common TCSs drift, which is close to the single TCS drift $T_0 - T$ per cavity round trip, the following procedure was used. The intensity time trace obtained through numerical solution of Equations (1)–(3) was split into consecutive intervals of equal duration T_0. Then, these intervals were associated with consecutive round trip numbers.

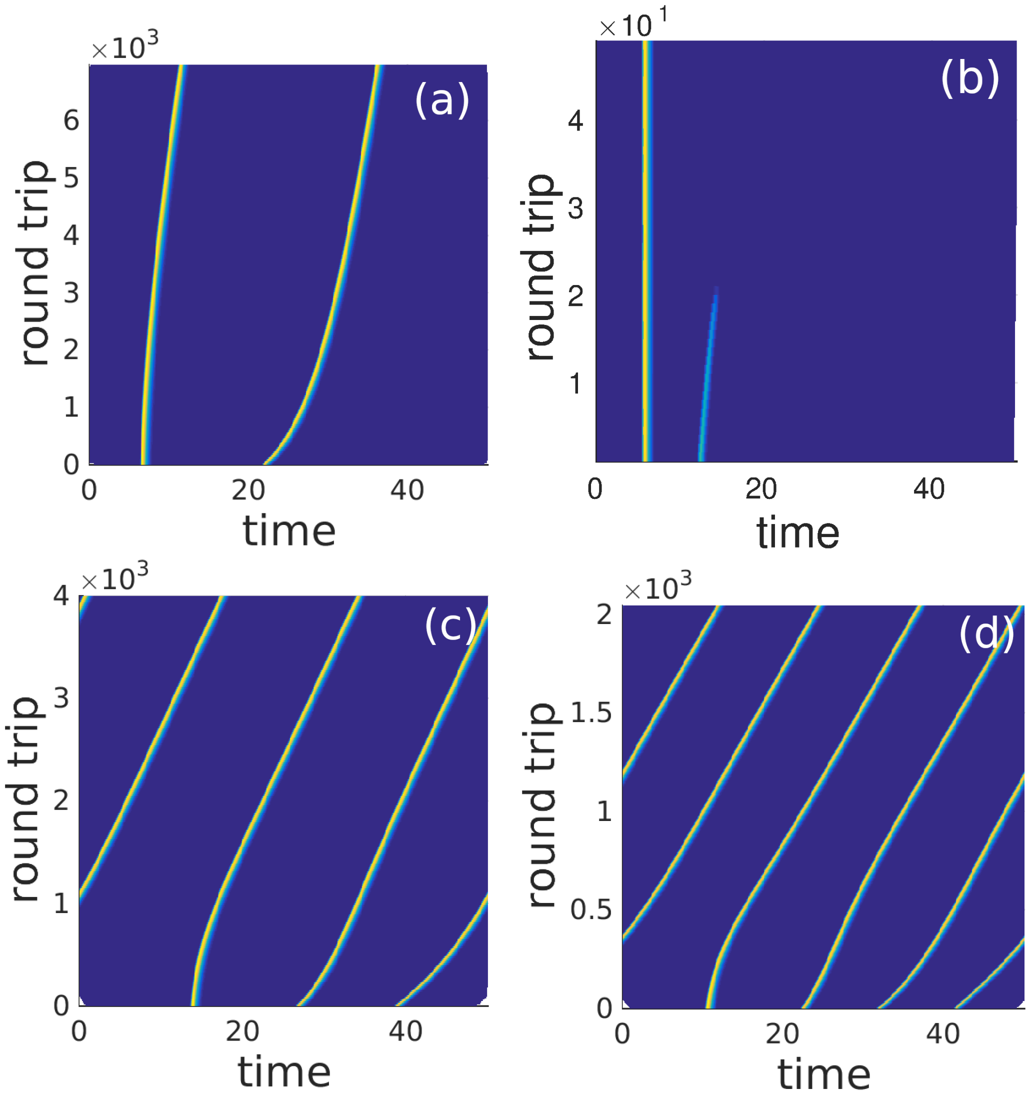

Figure 3. TSC repulsion due to the interaction via gain dynamics leading to a harmonic mode-locking regimes with two (**a**), three (**c**), and four (**d**) pulses per cavity round trip. Colorful lines indicate the trajectories of the interacting TCSs. Panel (**b**) illustrates repulsive interaction resulting in the annihilation of the second pulse. (**a**–**c**)—$g_0 = 0.5$. (**d**)—$g_0 = 0.8$. Cold cavity round trip time is $T = 50$. Other parameters are the same as in Figure 1.

The dependence of the interaction coefficient $K_{\tau g}$ on the linewidth enhancement factor in the gain section α_g is shown in Figure 4a. It is seen that this dependence is non-monotonic and has a pronounced resonant character. The interaction coefficient is negative (TCS repulsion) when the linewidth enhancement factor is sufficiently small, and it becomes positive (TCS attraction) with the increase in α_g, showing a sharp peak around $\alpha_g \approx 0.94$. A further increase in the α_g leads to a non-monotonic gradual decrease in the interaction coefficient, which becomes negative again at $\alpha_g \gtrsim 2.37$. The results of numerical simulations of Equations (1)–(3) with $\alpha_g = 2.0$ corresponding to a small positive values of the interaction coefficient are illustrated in Figure 5. It is seen that the interaction is very asymmetric; see refs. [15,21,26] and Appendix A. Figure 5b corresponding to $q_0 = 4.0$ and positive $K_{\tau g} \approx 0.854 \times 10^{-2}$ shows the TCS attraction leading to the merging of two pulses when one of them disappears after collision. In Figure 5a obtained for $q_0 = 5.0$ and $K_{\tau g} \approx 1.076 \times 10^{-2}$ the soliton attraction leads to a formation of a pulse bound state. Since for $\alpha_g \neq 0$, the relation $d_3 = d_4 = 0$ does not hold any more, the TCS phases are evolving with time in the course of interaction. Therefore, the bound state shown in Figure 5a is similar to the "incoherent" bound state described in [21] with the phase difference $\Delta\phi$ between two pulses growing monotonically with time (see Figure 6 illustrating the intensity time trace and the evolution of the TCS phase difference of the incoherent bound state). It was demonstrated in [21] that due to the electric field overlap of the interacting TCS, such types of bound states are characterized by slightly oscillating time separation $\Delta\tau$. However, since the interaction via electric fields is extremely weak, for the bound state shown in Figure 5a, such oscillation is hardy possible to detect. Figure 4b shows the evolution of the inter-soliton time separation $\Delta\tau$ as a function of the round trip number obtained via direct numerical simulation of the laser model (1)–(3). The parameter values are the same as in Figure 4a. It is seen that for $\alpha_g = 0.5$, when the interaction coefficient $K_{\tau g}$ is negative, the TCS interaction is repulsive and leads to a harmonic mode-locking regime. On the contrary, for $\alpha_g = 1.0, 1.5, 2.0$, which correspond to $K_{\tau g} > 0$, the interaction results in the formation of a pulse bound state. Furthermore, comparing Figure 4b with Figure 4a, we can see that the smaller the interaction coefficient, the weaker the interaction force and, hence, the longer the transient time before the equilibrium inter-pulse time separation is achieved. The final inter-pulse distance in the bound state is, however, almost independent of α_g and $K_{\tau g}$. Note that the time separation of the pulses in the incoherent bound state shown in Figure 5a is of the same order of magnitude as the gain relaxation time. This is why the pulses in this bound state have significantly different peak powers (see Figure 6a) and cannot be considered as individual TCSs any more. Therefore, the interaction Equations (16) and (17) are not valid when the pulses are so close to one another. Indeed, in order for a bound state to be formed, the attraction predicted by the interaction equations should be compensated by a repulsion at sufficiently small inter-pulse distances. This repulsion dominating at small pulse separations might be related to the pulse repulsion in a laser with a cavity round trip time shorter or much shorter than the gain relaxation time discussed in [11,13].

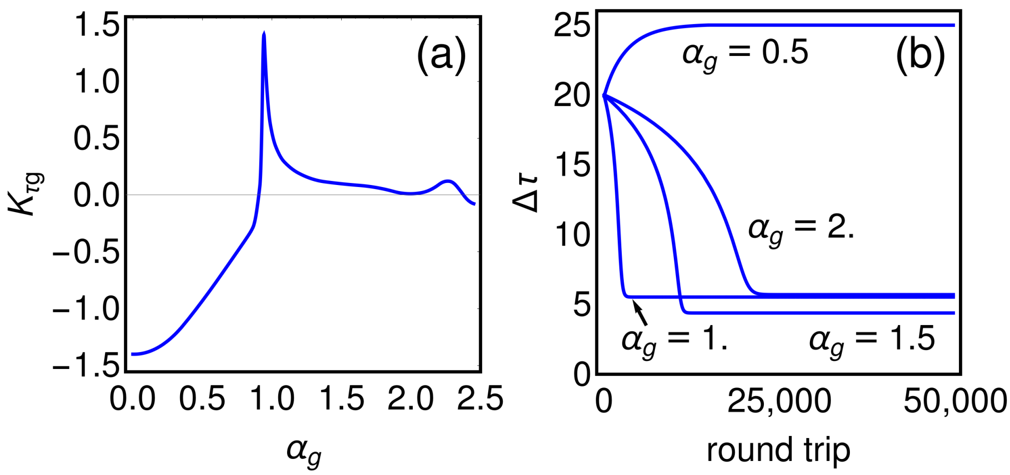

Figure 4. Interaction coefficient $K_{\tau g}$ as a function of α_g (**a**) and pulse time separation as a function of the round trip number (**b**). Different curves in panel (**b**) correspond to different linewidth enhancement factor values, $\alpha_g = 0.5, 1.0, 1.5, 2.0$, as indicated in the panel. $g_0 = 0.8$. Other parameters are the same as in Figure 1.

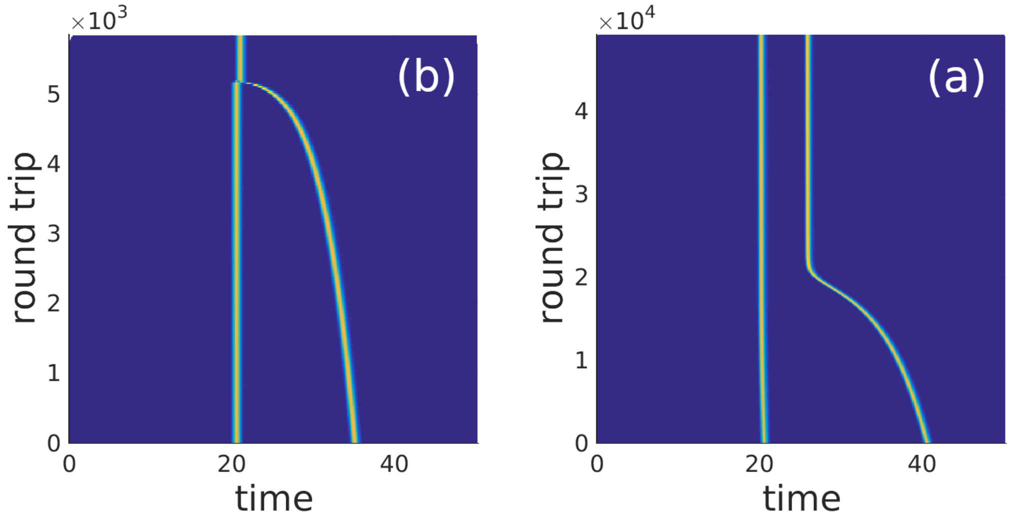

Figure 5. TCS interaction resulting in pulse bound state formation at $q_0 = 5.0$ (**a**) and pulse merging at $q_0 = 4.0$ (**b**). Colorful lines indicate the trajectories of the interacting TCSs. $g_0 = 0.8$, $\alpha_g = 2.0$, $\alpha_q = 0$. The cold cavity round trip time is $T = 50$. Other parameters are as shown in Figure 3.

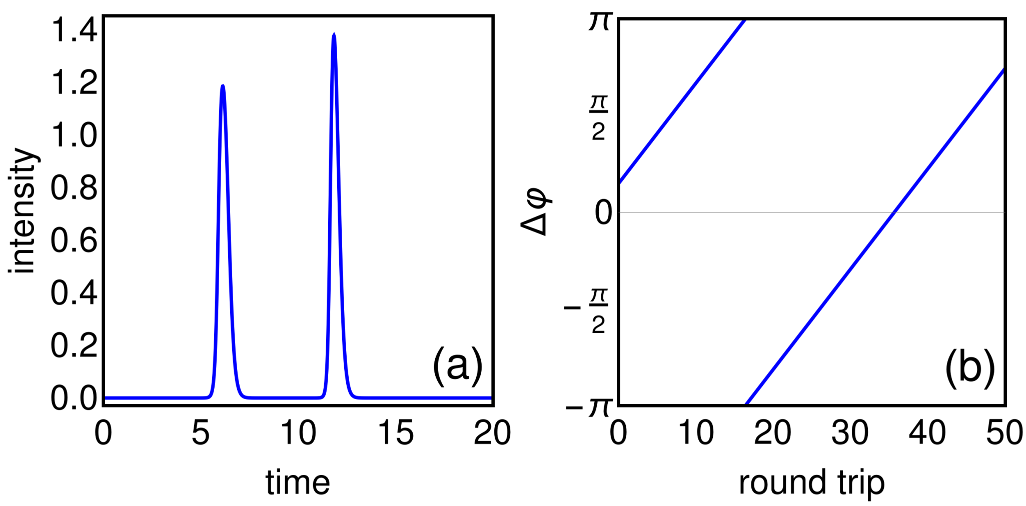

Figure 6. Intensity time-trace (**a**) and pulse phase difference (**b**) of the TCS bound state. Parameters are the same as in Figure 5a.

6. Conclusions

The interactions of two well-separated TCSs in a long cavity semiconductor laser were studied numerically and analytically using the DDE mode-locking model. Interaction equations governing the slow evolution of the time separation and phase difference of the TCSs were derived and analyzed in the parameter range typical of semiconductor lasers, where the interaction via the gain saturation and recovery dominates over the interaction via absorption and field dynamics. Analytical results were compared to direct numerical simulations of the DDE mode-locking model. It was demonstrated that in addition to usual pulse repulsion predicted in [11,13], an attractive TCS interaction is also possible in a laser with a nonzero linewidth enhancement factor. This attractive interaction can result either in pulse merging or in a formation of an incoherent pulse bound state. In the latter case, the repulsion force counteracting the soliton attraction force might be attributed to the standard mechanism of the mode-locking pulse repulsion described in [11,13], which acts beyond the TCS limit. The incoherent bound pulse state discussed here is similar to that observed experimentally [29] and described theoretically [21] in a nonlinear mirror mode-locked laser. It is also similar to the "type A" pulse bound states reported in [12]. The mechanism of the latter bound states formation is, however, different from that described here and can be related to the TCS attraction due to the interaction via the absorption component of the pulsed solution in a laser with an infinitely large gain relaxation time.

Funding: This research was funded by the Deutsche Forschungsgemeinschaft (DFG projects No. 445430311 and No. 491234846).

Data Availability Statement: Not applicable.

Conflicts of Interest: The author declares no conflict of interest.

Appendix A. Derivation of the Interaction Equations

Substituting Equation (13) into Equation (4), collecting the first order terms in small parameter ϵ, and applying the solvability conditions [30] to the resulting equation yield

$$\partial_t \tau_k = -\left\langle \boldsymbol{\theta}_k^\dagger \cdot \mathbf{P} \right\rangle, \quad \partial_t \phi_k = -\left\langle \boldsymbol{\varphi}_k^\dagger \cdot \mathbf{P} \right\rangle, \tag{A1}$$

$$\mathbf{P} = -\,\partial_t \mathbf{u}_\Sigma + \mathbf{F}_{\omega_0}(\mathbf{u}_\Sigma) + \mathbf{H}_{\omega_0}[\mathbf{u}_\Sigma(t-T)], \tag{A2}$$

where $\mathbf{u}_\Sigma = \mathbf{u}_1 + \mathbf{u}_2$, $\langle \cdot \rangle = \int_0^{T_0} \cdot dt$ and $\boldsymbol{\theta}_k^\dagger$ ($\boldsymbol{\varphi}_k^\dagger$) is the adjoint translational (phase) neutral mode evaluated on $\mathbf{u}_k$, $k = 1, 2$.

Since $\mathbf{u}_k$ is the solution of Equation (4), the equality

$$\sum_{k=1}^{2} \{-\partial_t \mathbf{u}_k + \mathbf{F}_{\omega_0}(\mathbf{u}_k) + \mathbf{H}_{\omega_0}[\mathbf{u}_k(t-T)]\} = 0$$

is satisfied. Subtracting this equality from (A2) we get

$$\mathbf{P} = \mathbf{F}_{\omega_0}(\mathbf{u}_\Sigma) - \sum_{k=1}^{2} \mathbf{F}_{\omega_0}(\mathbf{u}_k) + \mathbf{H}_{\omega_0}[\mathbf{u}_\Sigma(t-\tau)] - \sum_{k=1}^{2} \mathbf{H}_{\omega_0}[\mathbf{u}_k(t-T)].$$

Therefore, the equation for τ_2 in (A1) is

$$\begin{aligned} \partial_t \tau_2 = -\left\langle \boldsymbol{\theta}_2^\dagger \cdot \mathbf{P} \right\rangle = -\Bigg\langle \boldsymbol{\theta}_2^\dagger \cdot \Bigg\{ & \mathbf{F}_{\omega_0}(\mathbf{u}_\Sigma) - \sum_{k=1}^{2} \mathbf{F}_{\omega_0}(\mathbf{u}_k) \\ & + \mathbf{H}_{\omega_0}[\mathbf{u}_\Sigma(t-T)] - \sum_{k=1}^{2} \mathbf{H}_{\omega_0}[\mathbf{u}_k(t-T)] \Bigg\} \Bigg\rangle. \end{aligned} \tag{A3}$$

Using T_0 periodicity of $\boldsymbol{\theta}_2^\dagger$ and $\mathbf{u}_{1,2}$, Equation (A3) can be rewritten as

$$\begin{aligned} \partial_t \tau_2 = & -\left\langle \boldsymbol{\theta}_2^\dagger \cdot \left[\mathbf{F}_{\omega_0}(\mathbf{u}_\Sigma) - \sum_{k=1}^{2} \mathbf{F}_{\omega_0}(\mathbf{u}_k) \right] \right\rangle \\ & -\left\langle \boldsymbol{\theta}_2^\dagger(t+T) \cdot \left[\mathbf{H}_{\omega_0}(\mathbf{u}_\Sigma) - \sum_{k=1}^{2} \mathbf{H}_{\omega_0}(\mathbf{u}_k) \right] \right\rangle. \end{aligned} \tag{A4}$$

Next, we split the integral $\langle \cdot \rangle = \int_0^{T_0} \cdot dt$ into two parts $\langle \cdot \rangle = \langle \cdot \rangle_1 + \langle \cdot \rangle_2$, where $\langle \cdot \rangle_1 = \int_{-T_0/2}^{0} \cdot dt$ and $\langle \cdot \rangle_2 = \int_0^{T_0/2} \cdot dt$ are the integrals over the intervals $[-T_0/2, 0]$ and $[0, T_0/2]$, respectively:

$$
\begin{aligned}
\partial_t \tau_2 &= -\sum_{j=1}^{2} \left\langle \boldsymbol{\theta}_2^\dagger \cdot \left[\mathbf{F}_{\omega_0}(\mathbf{u}_\Sigma) - \sum_{k=1}^{2} \mathbf{F}_{\omega_0}(\mathbf{u}_k) \right] \right\rangle_j \\
&- \sum_{j=1}^{2} \left\langle \boldsymbol{\theta}_2^\dagger(t+T) \cdot \left[\mathbf{H}_{\omega_0}(\mathbf{u}_\Sigma) - \sum_{k=1}^{2} \mathbf{H}_{\omega_0}(\mathbf{u}_k) \right] \right\rangle_j .
\end{aligned}
$$

On the first interval $[-T_0/2, 0]$, where $\mathbf{u}_2$ is small, one obtains

$$
\mathbf{F}_{\omega_0}(\mathbf{u}_\Sigma) - \mathbf{F}_{\omega_0}(\mathbf{u}_1) \approx \mathcal{B}_1 \mathbf{u}_2, \quad \mathbf{H}_{\omega_0}(\mathbf{u}_\Sigma) - \mathbf{H}_{\omega_0}(\mathbf{u}_1) \approx \mathcal{C}_1 \mathbf{u}_2,
$$

and

$$
\mathbf{F}_{\omega_0}(\mathbf{u}_2) \approx \mathcal{B}_0 \mathbf{u}_2, \quad \mathbf{H}_{\omega_0}(\mathbf{u}_2) \approx \mathcal{C}_0 \mathbf{u}_2
$$

where $\mathcal{B}_1 = \mathcal{B}(\mathbf{u}_1)$ and $\mathcal{C}_1 = \mathcal{C}(\mathbf{u}_1)$ $[\mathcal{B}_0 = \mathcal{B}(0)$ and $\mathcal{C}_0 = \mathcal{C}(0)]$ are the linearization matrices of $\mathbf{F}_{\omega_0}(\mathbf{U})$ and $\mathbf{H}_{\omega_0}(\mathbf{U})$ at $\mathbf{U} = \mathbf{u}_1$ $(\mathbf{U} = 0)$. Similarly, on the second interval $[0, T_0/2]$, where $\mathbf{u}_1$ is small, one gets

$$
\mathbf{F}_{\omega_0}(\mathbf{u}_\Sigma) - \mathbf{F}_{\omega_0}(\mathbf{u}_2) \approx \mathcal{B}_2 \mathbf{u}_1, \quad \mathbf{H}_{\omega_0}(\mathbf{u}_\Sigma) - \mathbf{H}_{\omega_0}(\mathbf{u}_1) \approx \mathcal{C}_2 \mathbf{u}_1,
$$

where $\mathcal{B}_2 = \mathcal{B}(\mathbf{u}_2)$ and $\mathcal{C}_2 = \mathcal{C}(\mathbf{u}_2)$ and

$$
\mathbf{F}_{\omega_0}(\mathbf{u}_1) \approx \mathcal{B}_0 \mathbf{u}_1, \quad \mathbf{H}_{\omega_0}(\mathbf{u}_2) \approx \mathcal{C}_0 \mathbf{u}_1. \tag{A5}
$$

Consequently, one obtains

$$
\begin{aligned}
\partial_t \tau_2 &\approx -\left\langle \boldsymbol{\theta}_2^\dagger \cdot (\mathcal{B}_1 - \mathcal{B}_0) \mathbf{u}_2 \right\rangle_1 - \left\langle \boldsymbol{\theta}_2^\dagger(t+T) \cdot (\mathcal{C}_1 - \mathcal{C}_0) \mathbf{u}_2 \right\rangle_1 \\
&- \left\langle \boldsymbol{\theta}_2^\dagger \cdot \{(\mathcal{B}_2 - \mathcal{B}_0) \mathbf{u}_1\} \right\rangle_2 - \left\langle \boldsymbol{\theta}_2^\dagger(t+T) \cdot (\mathcal{C}_2 - \mathcal{C}_0) \mathbf{u}_1 \right\rangle_2,
\end{aligned}
$$

where the first two terms in the right hand side containing the product of two small quantities $\boldsymbol{\theta}_2^\dagger$ and $\mathbf{u}_2$ on the first interval $[-T_0/2, 0]$ can be neglected. This yields

$$
\partial_t \tau_2 \approx -\left\langle \boldsymbol{\theta}_2^\dagger \cdot (\mathcal{B}_2 - \mathcal{B}_0) \mathbf{u}_1 \right\rangle_2 - \left\langle \boldsymbol{\theta}_2^\dagger(t+T) \cdot (\mathcal{C}_2 - \mathcal{C}_0) \mathbf{u}_1 \right\rangle_2.
$$

Since $\mathbf{u}_1$ is the solution of Equation (4), it satisfies the equation $-\partial_t \mathbf{u}_1 + \mathbf{F}_{\omega_0}(\mathbf{u}_1) + \mathbf{H}_{\omega_0}[\mathbf{u}_1(t-T)] = 0$. Using the relations (A5) valid on the second interval $[0, T_0/2]$, one can rewrite it in the form

$$
-\partial_t \mathbf{u}_1 + \mathcal{B}_0 \mathbf{u}_1 + \mathcal{C}_0 \mathbf{u}_1(t-T) \approx 0. \tag{A6}
$$

The adjoint neutral mode $\boldsymbol{\theta}_2^\dagger$ satisfies the equation

$$
\partial_t \boldsymbol{\theta}_2^\dagger + \boldsymbol{\theta}_2^\dagger \mathcal{B}_2 + \boldsymbol{\theta}_2^\dagger(t+T) \mathcal{C}_2 = 0. \tag{A7}
$$

Multiplying Equation (A7) by $\mathbf{u}_1$, subtracting from the resulting equation Equation (A6) multiplied by $\boldsymbol{\theta}_2^\dagger$, and integrating over the second interval $[0, T_0/2]$, one gets

$$
\begin{aligned}
\left\langle \boldsymbol{\theta}_2^\dagger \cdot (\mathcal{B}_2 - \mathcal{B}_0) \mathbf{u}_1 \right\rangle_2 &\approx -\left\langle \partial_t \boldsymbol{\theta}_2^\dagger \cdot \mathbf{u}_1 + \boldsymbol{\theta}_2^\dagger \cdot \partial_t \mathbf{u}_1 \right\rangle_2 \\
&- \left\langle \boldsymbol{\theta}_2^\dagger(t+T) \mathcal{C}_2 \cdot \mathbf{u}_1 - \boldsymbol{\theta}_2^\dagger \cdot \mathcal{C}_0 \mathbf{u}_1(t-T) \right\rangle_2.
\end{aligned}
$$

Substitution of this relation into (A6) gives

$$
\begin{aligned}
\partial_t \tau_2 \approx \left\langle \partial_t \boldsymbol{\theta}_2^\dagger \cdot \mathbf{u}_1 + \boldsymbol{\theta}_2^\dagger \cdot \partial_t \mathbf{u}_1 \right\rangle_2 + \Big\langle \boldsymbol{\theta}_2^\dagger(t+T) \mathcal{C}_2 \cdot \mathbf{u}_1 \\
- \boldsymbol{\theta}_2^\dagger \cdot \mathcal{C}_0 \mathbf{u}_1(t-T)_2 - \boldsymbol{\theta}_2^\dagger(t+T) \cdot (\mathcal{C}_2 - \mathcal{C}_0) \mathbf{u}_1 \Big\rangle_2.
\end{aligned}
$$

Finally, integrating the full derivative $\partial_t \left(\boldsymbol{\theta}_2^\dagger \cdot \mathbf{u}_1 \right)$ over the interval $[0, T_0/2]$ leads to

$$\begin{aligned} \partial_t \tau_2 \quad &\approx \quad \boldsymbol{\theta}_2^\dagger(T_0/2)\mathbf{u}_1(T_0/2) - \boldsymbol{\theta}_2^\dagger(0)\mathbf{u}_1(0) \\ &+ \quad \left\langle \boldsymbol{\theta}_2^\dagger(t+T) \cdot \mathcal{C}_0 \mathbf{u}_1 - \boldsymbol{\theta}_2^\dagger \mathcal{C}_0 \cdot \mathbf{u}_1(t-T) \right\rangle_2. \end{aligned} \tag{A8}$$

Note, that all the elements of the 4×4 matrix $\mathcal{C}_0$ are equal to zero, except those in the upper 2×2 diagonal block. Hence, the last term in Equation (A8),

$$\begin{aligned} &\left\langle \boldsymbol{\theta}_2^\dagger(t+T) \cdot \mathcal{C}_0 \mathbf{u}_1 - \boldsymbol{\theta}_2^\dagger \mathcal{C}_0 \cdot \mathbf{u}_1(t-T) \right\rangle_2 \\ &= -\left(\int_0^\delta + \int_{T/2}^{T/2+\delta} \right) \left[\boldsymbol{\theta}_2^\dagger(t+T)\mathcal{C}_0 \mathbf{u}_1 \right] dt, \end{aligned}$$

contains only the asymptotic expressions for the field components, which are assumed to be small and are neglected in this study. Therefore, we can drop the last term in Equation (A8).

The equation for slow evolution of τ_1 is derived in a similar way to Equation (A8):

$$\begin{aligned} &\partial_t \tau_1 \approx \boldsymbol{\theta}_1^\dagger(0)\mathbf{u}_2(0) - \boldsymbol{\theta}_1^\dagger(T_0/2)\mathbf{u}_2(T_0/2) \\ &+ \left\langle \boldsymbol{\theta}_1^\dagger(t+T) \cdot \mathcal{C}_0 \mathbf{u}_2 - \boldsymbol{\theta}_1^\dagger \mathcal{C}_0 \cdot \mathbf{u}_2(t-T) \right\rangle_1. \end{aligned} \tag{A9}$$

Note, that the terms $\boldsymbol{\theta}_2^\dagger(T_0/2)\mathbf{u}_1(T_0/2)$ and $\boldsymbol{\theta}_1^\dagger(0)\mathbf{u}_2(0)$ in Equations (A8) and (A9), respectively, can be neglected due to the fast decay of the leading tail of the TCS solution and trailing edge of the adjoint neutral mode. The remaining terms, $\boldsymbol{\theta}_2^\dagger(0)\mathbf{u}_1(0)$ in Equation (A8) and $\boldsymbol{\theta}_1^\dagger(T_0/2)\mathbf{u}_2(T_0/2)$ in Equation (A9), have very different magnitudes except for the case, where the TCSs are nearly equidistant in the cavity, $\Delta\tau = \tau_2 - \tau_1 \approx \tau_0/2$. This means that except for this case the TCS interaction is strongly asymmetric and does not satisfy Newton's third law [15,21,26]. Thus, keeping only the second terms in the right hand sides of Equations (A8) and (A9), one gets the following equation for the TCS time separation $\Delta\tau = \tau_2 - \tau_1$:

$$\partial_t \Delta\tau \approx \boldsymbol{\theta}_1^\dagger(T_0/2)\mathbf{u}_2(T_0/2) - \boldsymbol{\theta}_2^\dagger(0)\mathbf{u}_1(0). \tag{A10}$$

The equation for the slow evolution of the phase difference $\Delta\phi = \phi_2 - \phi_1$ can be derived in a similar way. This equation reads:

$$\partial_t \Delta\phi \approx \boldsymbol{\varphi}_1^\dagger(T_0/2)\mathbf{u}_2(T_0/2) - \boldsymbol{\varphi}_2^\dagger(0)\mathbf{u}_1(0). \tag{A11}$$

References

1. Grelu, P.; Akhmediev, N. Dissipative solitons for mode-locked lasers. *Nat. Photonics* **2012**, *6*, 84–92. [CrossRef]
2. Herr, T.; Brasch, V.; Jost, J.D.; Wang, C.Y.; Kondratiev, N.M.; Gorodetsky, M.L.; Kippenberg, T.J. Temporal solitons in optical microresonators. *Nat. Photonics* **2014**, *8*, 145–152. [CrossRef]
3. Kippenberg, T.J.; Gaeta, A.L.; Lipson, M.; Gorodetsky, M.L. Dissipative Kerr solitons in optical microresonators. *Science* **2018**, *361*, 6402. [CrossRef]
4. Marconi, M.; Javaloyes, J.; Balle, S.; Giudici, M. How lasing localized structures evolve out of passive mode locking. *Phys. Rev. Lett.* **2014**, *112*, 223901. [CrossRef]
5. Rosanov, N.; Khodova, G. Diffractive autosolitons in nonlinear interferometers. *J. Opt. Soc. Am. B* **1990**, *7*, 1057–1065. [CrossRef]
6. Malomed, B.A. Bound states of envelope solitons. *Phys. Rev. E* **1993**, *47*, 2874. [CrossRef] [PubMed]
7. Akhmediev, N.; Ankiewicz, A.; Soto-Crespo, J. Multisoliton solutions of the complex Ginzburg-Landau equation. *Phys. Rev. Lett.* **1997**, *79*, 4047. [CrossRef]
8. Akhmediev, N.; Rodrigues, A.S.; Town, G.E. Interaction of dual-frequency pulses in passively mode-locked lasers. *Opt. Commun.* **2001**, *187* 419–426. [CrossRef]
9. Vladimirov, A.G.; Khodova, G.V.; Rosanov, N.N. Stable bound states of one-dimensional autosolitons in a bistable laser. *Phys. Rev. E* **2001**, *63*, 056607. [CrossRef] [PubMed]
10. Ablowitz, M.J.; Horikis, T.P.; Nixon, S.D. Soliton strings and interactions in mode-locked lasers. *Opt. Commun.* **2009**, *282*, 4127–4135. [CrossRef]
11. Kutz, J.N.; Collings, B.; Bergman, K.; Knox, W. Stabilized pulse spacing in soliton lasers due to gain depletion and recovery. *IEEE J. Quantum Electron.* **1998**, *34*, 1749–1757. [CrossRef]

12. Soto-Crespo, J.M.; Akhmediev, N.N. Multisoliton regime of pulse generation by lasers passively mode locked with a slow saturable absorber. *J. Opt. Soc. Am. B* **1999**, *16*, 674–677. [CrossRef]
13. Nizette, M.; Rachinskii, D.; Vladimirov, A.; Wolfrum, M. Pulse interaction via gain and loss dynamics in passive mode locking. *Phys. D* **2006**, *218*, 95–104. [CrossRef]
14. Zaviyalov, A.; Grelu, P.; Lederer, F. Impact of slow gain dynamics on soliton molecules in mode-locked fiber lasers. *Opt. Lett.* **2012**, *37*, 175–177. [CrossRef]
15. Camelin, P.; Javaloyes, J.; Marconi, M.; Giudici, M. Electrical addressing and temporal tweezing of localized pulses in passively-mode-locked semiconductor lasers. *Phys. Rev. A* **2016**, *94*, 063854. [CrossRef]
16. Vladimirov, A.G.; Turaev, D. Model for passive mode locking in semiconductor lasers. *Phys. Rev. A* **2005**, *72*, 033808. [CrossRef]
17. Vladimirov, A.G.; Turaev, D.; Kozyreff, G. Delay differential equations for mode-locked semiconductor lasers. *Opt. Lett.* **2004**, *29*, 1221–1223. [CrossRef]
18. Vladimirov, A.G.; Turaev, D. New model for mode-locking in semiconductor lasers. *Radiophys. Quant. Electron.* **2004**, *47*, 857–865. [CrossRef]
19. Puzyrev, D.; Vladimirov, A.G.; Pimenov, A.; Gurevich, S.V.; Yanchuk, S. Bound pulse trains in arrays of coupled spatially extended dynamical systems. *Phys. Rev. Lett.* **2017**, *119*, 163901. [CrossRef] [PubMed]
20. Munsberg, L.; Javaloyes, J.; Gurevich, S.V. Topological localized states in the time delayed Adler model: Bifurcation analysis and interaction law. *Chaos* **2020**, *30*, 063137. [CrossRef]
21. Vladimirov, A.G. Short-and long-range temporal cavity soliton interaction in delay models of mode-locked lasers. *Phys. Rev. E* **2022**, *105*, 044207. [CrossRef]
22. Vladimirov, A.G.; Kovalev, A.V.; Viktorov, E.A.; Rebrova, N.; Huyet, G. Dynamics of a class-A nonlinear mirror mode-locked laser. *Phys. Rev. E* **2019**, *100*, 012216. [CrossRef] [PubMed]
23. Yanchuk, S.; Ruschel, S.; Sieber, J.; Wolfrum, M. Temporal dissipative solitons in time-delay feedback systems. *Phys. Rev. Lett.* **2019**, *123*, 053901. [CrossRef] [PubMed]
24. Stöhr, M.; Wolfrum, M. Temporal dissipative solitons in the Morris–Lecar model with time-delayed feedback. *Chaos* **2023**, *33*, 023117. [CrossRef]
25. Turaev, D.; Vladimirov, A.G.; Zelik, S. Long-range interaction and synchronization of oscillating dissipative solitons. *Phys. Rev. Lett.* **2012**, *108*, 263906. [CrossRef] [PubMed]
26. Vladimirov, A.G.; Gurevich, S.V.; Tlidi, M. Effect of Cherenkov radiation on localized-state interaction. *Phys. Rev. A* **2018**, *97*, 013816. [CrossRef]
27. Vladimirov, A.G.; Tlidi, M.; Taki, M. Dissipative soliton interaction in Kerr resonators with high-order dispersion. *Phys. Rev. A* **2021**, *103*, 063505. [CrossRef]
28. Guglielmi, N.; Hairer, E. Implementing Radau IIA methods for stiff delay differential equations. *Computing* **2001**, *67*, 1–12. [CrossRef]
29. Kokhanovskiy, A.; Kuprikov, E.; Kobtsev, S. Single-and multi-soliton generation in figure-eight mode-locked fibre laser with two active media. *Opt. Laser Technol.* **2020**, *131*, 106422. [CrossRef]
30. Halanay, A. *Differential Equations: Stability, Oscillations, Time Lags*; Academic Press: New York, NY, USA, 1966; Volume 23.